Colloids and Surfaces A: Physicochemical and Engineering Aspects 679 (2023) 132575

Contents lists available at ScienceDirect

Colloids and Surfaces A: Physicochemical and Engineering Aspects

journal homepage: www.elsevier.com/locate/colsurfa

Surfactant transport upon foam films moving through porous media

Paul Grassia [a,*], Hamed Rajabi [a], Ruben Rosario [a], Carlos Torres-Ulloa [a,b,c]

[a] Department of Chemical and Process Engineering, University of Strathclyde, James Weir Building, 75 Montrose Street, Glasgow, G1 1XQ, UK
[b] Centro de Investigación, Innovación y Creación (CIIC), Universidad Católica de Temuco, Rudecindo Ortega 03690, Temuco, Chile
[c] Departamento de Ciencias Matemáticas y Físicas, Facultad de Ingeniería, Universidad Católica de Temuco, Rudecindo Ortega 03690, Temuco, Chile

HIGHLIGHTS

- Foam films stretching or shrinking as they move through porous media are considered.
- Surfactant surface concentration on the stretching or shrinking films is modelled.
- For high stretch rates or large amounts of stretch, concentration falls very low.
- For shrinking films, surfactant concentration is non-monotonic with film length.
- Either uniform, quasistatic or boundary layer solutions possible in various regimes.

GRAPHICAL ABSTRACT

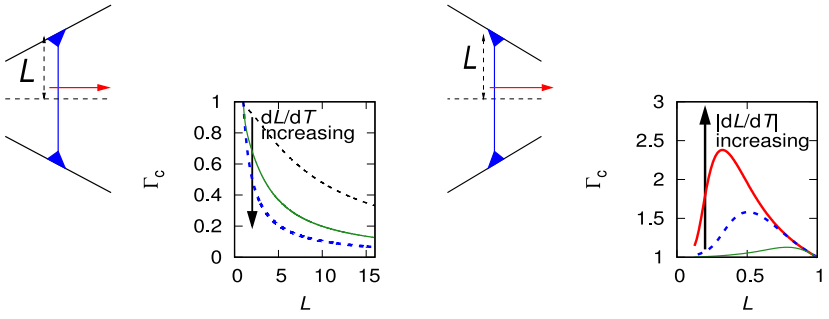

ARTICLE INFO

Dataset link: https://doi.org/10.15129/2a588cdd-68a5-45c7-b267-dd15243bc5a3

Keywords:
Foam films in porous media
Stretching/shrinking
Marangoni flow
Surfactant surface concentration
Mathematical modelling
Asymptotic solutions

ABSTRACT

In the context of foam improved oil recovery or foam-based soil/aquifer remediation, a model is presented for evolution of surfactant surface concentration on foam films moving through porous media. The model exploits an analogy between surface transport behaviour in foam fractionation and surfactant transport behaviour for foam in porous media. Films either stretch as they move from pore throat to pore body, or shrink when moving from pore body to pore throat: this stretching/shrinking then influences surfactant concentration. In addition, Plateau borders at the edges of films can supply surfactant to films, or receive surfactant from them. The model is solved numerically and key parameters governing its behaviour are identified. Parameter regimes are encountered, corresponding to modest stretching or shrinkage rates, in which surfactant concentration on films is predicted to be closely coupled to surfactant concentration in Plateau borders. Alternate parameter regimes are encountered, corresponding instead to fast stretching or shrinkage rates, in which surfactant concentration on films is predicted to become independent of surfactant concentration in Plateau borders. Asymptotic solutions available in each of these regimes are compared with numerical solutions. A preliminary comparison between the model predictions and experimental data from literature is also described. The appeal of the model is that predictions can be made comparatively simply. Indeed the model can predict when foam films might become significantly depleted in surfactant, possibly leaving films liable to breakage, which would then be detrimental to foam in porous media applications.

1. Introduction

Flow of foam films within porous media, including within model porous media, has been a topic of interest over many years (see e.g. [1] as well as various more recent works [2–11]). The motivation for studying this topic is that there are engineering and environmental applications which involve foam moving through porous media [12]. These applications include foam improved oil recovery [13–19] and also environmental remediation of soils and of aquifers [20–29].

* Corresponding author.
E-mail address: paul.grassia@strath.ac.uk (P. Grassia).

https://doi.org/10.1016/j.colsurfa.2023.132575
Received 30 June 2023; Received in revised form 10 October 2023; Accepted 11 October 2023
Available online 17 October 2023

Yet another application is foaming of carbon dioxide for carbon capture [30,31]. To take foam improved oil recovery as an example, one study [32] showed that oil recovery increased dramatically by as much as 70% of original oil in place when water flooding was replaced by foam flooding. Another study [33] comparing gas flooding with foam flooding found an increase in recovery by up to 49% of original oil in place. Field trials [34] found that use of foam increased oil recovery from a particular well by around 30% or so (a figure computed here by comparing the increased production over the entire foam trial period, the duration of the trial period, and the typical daily production rate immediately prior to the use of foam).

All the above sorts of applications rely on the fact that (compared to single phase fluids) foam films have limited mobility in porous media [14,16,17,35–38]: as a result, foam can be used for flow control. Indeed control over the foam flow [39] should control the flow overall. The use of foam for flow control relies however upon foam films remaining stable within the media through which they move: if the foam films collapse within the medium [40], then benefits of using foam in oil recovery or environmental remediation applications cannot be realised. Indeed foam within porous media controls overall flow specifically because foam mobility is low. Gas that is left behind after foam collapses is much more mobile, and hence less effective at flow control [14].

Foam films can be stretched and/or contracted as they move [41]. Specifically films are stretched as they move from pore throats to pore bodies, but then are contracted again as they move from pore bodies into subsequent throats [42–47], and all of this may then impact film stability. Indeed some previous studies [48,49] (see also a relevant review [50]) considered a network model of foam with films in the network stretching (or shrinking) as the foam moved: within the network model, stretching in particular could lead to instability. To obtain a more in depth understanding of instability behaviour however, the starting point should be a single foam film in a single pore.

When any single moving film is subjected to stretching or shrinking, one important factor that affects foam film stability is the surfactant concentration [36–38,51–53]. The concentration of surfactant adsorbed on the surface is especially important, as it may affect surface mobility and also disjoining pressure, which in turn impact foam film stability [54–56]. What is found is that the lower the surfactant concentration, the less stable a foam film will be [38,52,53,57–59]: a stretched film in particular is liable to become depleted of surfactant [60–62]. Consequently stretch of individual films performed in a well controlled way [63–66] can be used to probe how stable or unstable such films might be [67–69]. Knowing how surfactant is transported along a foam film, is then relevant for understanding the stability of that film as it stretches or shrinks whilst moving through porous media say. This then is the topic to be studied here.

As noted above, the surface of a particular film might become depleted in surfactant as that film stretches, the reduction in surfactant concentration on a film making it less stable and hence more liable to break [38,57]. In porous media applications, this effect would be exacerbated if surfactant were to adsorb on the pore walls [34] as that would deplete surfactant in the film even further (although note that adsorption on pore walls is not to be considered here; only depletion due to stretching is considered). On the other hand, a film that shrinks might accumulate surfactant on its surface, making it more stable against breakage. That then would mitigate against any surfactant adsorption on pore walls (albeit, as mentioned, adsorption on walls is not considered here).

Describing surfactant transport on the surface of a film (even on a film which is not necessarily stretching or shrinking) can however in itself be a complicated topic [70–72]. Any non-uniformities in surfactant on the surface lead to spatial gradients in surface tension. These in turn drive so called Marangoni flows, which can exhibit rather complex flow fields [72]. Characterising the Marangoni flows and how they move surfactant around is therefore an essential part of describing surfactant transport on a film, and so must be tackled here.

Stretching or shrinking of films when this is present is coupled to the aforementioned Marangoni surfactant transport: it is thereby the combined stretching/shrinking flow and Marangoni flow which transports surfactant, not just the stretching/shrinking flow on its own. Some studies in literature [73–75] (see also a brief commentary upon those studies [76]) looked for instance at coupled stretching/shrinking and Marangoni flows in a device which stretched certain foam films and contracted others. These various films meet one another at menisci (so called Plateau borders) and models were provided for surfactant flow from film to film around the borders [74], with analysis of these models having been carried out [77]. However the focus in these works has been upon transport near the menisci, with less focus on the remaining parts of a film further away.

Foam film stretching or shrinking in porous media (the topic of interest here) is not the only context in which surfactant transport between Plateau borders and films (and subsequently along films) takes place. Another context is foam fractionation, often used for surfactant enrichment or separations [58,78–84]. Comparatively simple models describing the various surfactant transport processes occurring on the film scale during fractionation have been developed in literature [85–87]. These models are very relevant to the present work, so some of the background underlying them is described below.

During the fractionation process, surfactant solution can drain downward under gravity through a network of Plateau borders [88,89]. Foam films meanwhile (upon which the previously mentioned works [85–87] specifically focus) rise up through the foam and can start off leaner in surfactant than surrounding Plateau borders. Surfactant is then transferred from the Plateau borders onto and along foam film surfaces due to Marangoni flows. Simultaneously there is a film drainage process occurring [72,85–87] with capillary suction driving liquid from foam films into Plateau borders, thereby causing the foam films to thin. Thinning of films is however in many ways analogous to stretching them, since to conserve liquid, stretching must be accompanied by film thinning. Hence there should be an analogy between film scale surfactant transport in foam fractionation (involving Marangoni flows and film *thinning*) and surfactant transport within foam in porous media applications (involving Marangoni flows and film *stretching*). This analogy has not been explored previously. Exploring it is however worthwhile: the simplicity that has been mentioned as being already embedded in previously studied models describing fractionation [85–87] should carry over to models involving film stretching/shrinking.

To summarise, the aim here to is take models already available in the context of fractionation [85–87], and adapt them to describe foam films that either stretch or shrink moving through porous media. Obtaining such models and analysing (numerically and also asymptotically in various limits) the behaviours that they predict both for stretching and shrinking films is therefore the novel contribution of the present work. Whilst the present study remains modelling based, it is noted that the models for film scale fluid flow, film deformation and surfactant transport to be obtained here remain simpler to implement than others existing in literature [48,72,90,91]. The simplicity, at least for making a preliminary assessment of how surfactant moves on stretched or shrinking films, is intended to be part of the appeal.

The rest of this work is laid out as follows. Section 2 outlines and analyses the model that we use. Then Section 3 presents and discusses model results. After that Section 4 considers a preliminary comparison between the predictions of the model developed here and experimental findings in literature. Finally Section 5 offers conclusions, as well as a future outlook for using the model.

2. Model

The model that we use is closely related to the one already discussed in literature [85] so we only sketch out the main physical ideas

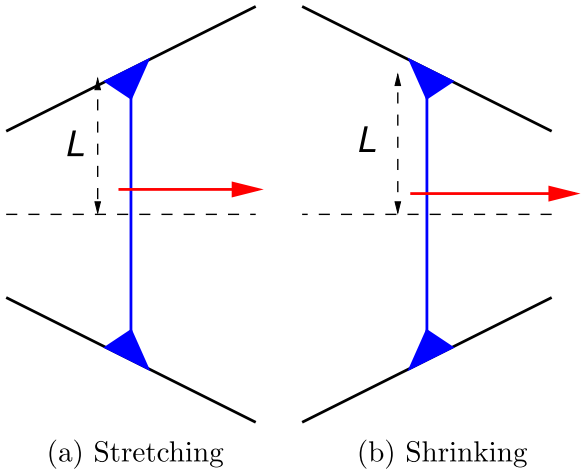

Fig. 1. A film (instantaneous half-length L) moving through a pore, and stretching or shrinking as it moves.

plus some key equations here. Further details of the model can be found in supplementary material (section S 1). The present section is laid out as follows. Section 2.1 considers the geometry of the film and the pore through which it moves. Then Sections 2.2–2.3 discuss surfactant surface concentration and surfactant transport. The main governing equation that we consider is introduced in Section 2.4: we emphasise that the equation derived here is novel, because even though stretching/shrinking and film thinning (as considered by previous work [85–87]) are related, they are not identical. Further details on this are discussed in the supplementary material (one significant difference being that stretching/shrinking rates imposed here can be rather larger than thinning rates due to film drainage on its own would be). After that in Sections 2.5–2.7 we present some novel asymptotic solutions to the governing equation. A numerical approach is described in Section 2.8.

2.1. Film and pore geometry

The geometric arrangement of a foam film within a pore that we consider is shown in Fig. 1. The pore is assumed symmetric about its centre line. The film spans the pore and has an instantaneous half-length L. Plateau borders (menisci) join the film to the pore wall. Film motion is from left to right. The pore widens moving to the right in Fig. 1(a) (stretching) but instead narrows moving to the right in Fig. 1(b) (shrinking). We consider a two-dimensional geometry here (i.e. a fixed breadth pore normal to the plane of Fig. 1) although the analysis we present could be generalised to an axisymmetric pore also (assuming of course that the film shape remains axisymmetric [90]).

In Fig. 1(a), the stretch rate of the film $\dot{L}$ (rate of change of the film half-length) is expected to be the product of the velocity at which the film is migrating along the pore and the tangent of the taper angle of the pore wall relative to the pore centre line. This assumes that individual elements on the film actually elongate as the film moves (instead of merely having new film extracted from the Plateau border). In general though, a combination of elongation and extraction could occur [92,93], but we focus in the first instance (up until Section 4) just on elongation (not extraction) here. If any extraction whatsoever is present, the product of film migration velocity and the tangent of the taper angle (in effect an imposed stretch rate) would become an upper bound for the true elongation rate. Conversely, were the model to be formulated in terms of an elongation rate (without accessing the film migration velocity directly), the ratio between the elongation rate and the tangent of the taper angle would be a lower bound for the film migration velocity. In fact what we do here is formulate just in terms of an imposed stretch rate, without direct reference to either migration velocity or taper angle, and assuming also that the true elongation rate matches that imposed stretch rate. In Fig. 1(b) meanwhile, the film is shrinking rather than stretching, so the value of $\dot{L}$ is negative.

Although film thickness can in principle vary spatially [94], films are treated here as being uniform thickness spatially, although that thickness is permitted to vary with time. Note also that in Fig. 1 the films are drawn as being flat, whereas in reality they are curved, typically bulging from the pore throat towards the pore body. Knowing about how the films bulge [42–47] is essential for determining the pressure required to drive them along. Here however we are considering not driving pressures but instead surfactant transport along the films. A model considering flat films [85–87] is therefore adequate here.

2.2. Surfactant surface concentration

In general surfactant can be present both dissolved within the bulk of foam films and also adsorbed on the surface of foam films. The more surface active that a surfactant is, and also the thinner that a film is, the greater the proportion of overall surfactant that is present in adsorbed form [86,87].

Here we assume (as has been done in some previous work [85]) that the dominant contribution is adsorbed surfactant on the foam film surface. This means that we only need to track surfactant adsorbed on the surface. Dissolved surfactant within the films can still be tracked in principle as has been done in prior work [86,87]. However that same work [86,87] demonstrated that it is indeed possible to consider a limiting case (approached either for sufficiently thin films or sufficiently low solubility surfactants) in which dissolved surfactant makes just a small contribution to the overall amount of surfactant that is present, and hence is neglected here, at least for films. Plateau borders however, being rather thicker than films may still have significant dissolved surfactant.

The model we study for films here considers therefore the spatiotemporal evolution of the adsorbed surfactant on the film surface: the variable we consider Γ is surfactant adsorbed per element of film area, or (in the two-dimensional model here with a specified pore breadth normal to the plane of Fig. 1) surfactant adsorbed per element of film length. In effect therefore, the quantity Γ measures surfactant surface concentration.

As alluded to earlier, despite considering here that surfactant on the film is dominated by adsorbed surfactant, there can still be significant dissolved surfactant in the adjacent Plateau borders (where the foam film meets the pore walls). This follows because (as Fig. 1 also indicates) Plateau borders can be much thicker than foam films, which means they potentially contain much more liquid than films themselves do [92]. Plateau borders can therefore be assumed to act as reservoirs of surfactant [85–87], and we employ the same assumption here.

2.3. Surfactant transport

Now we consider the mechanism of surfactant transport. Stretching a film as in Fig. 1(a) depletes it of surfactant (i.e. reduces the value of Γ, which here is the amount of surfactant per element of film length, as we have said). However since the edge of the film is in contact with a reservoir, the surfactant surface concentration right at the edge of the film where it meets the Plateau border cannot decrease. We therefore have a gradient of surfactant surface concentration between the edge of the film and regions further from the edge.

Since surface tension is a function of adsorbed surfactant surface concentration (low surfactant surface concentration away from the edges gives higher surface tension) a gradient of surface tension is now present. This gradient of surface tension implies a shear stress (a so called Marangoni stress) at the film surface. This then produces, as alluded to within the introduction, a Marangoni flow.

Computing such a flow in detail requires knowledge of any non-uniformities in film thickness [72,90]. However previous work [85–87] made an approximation that the film could be treated as having roughly uniform thickness as Section 2.1 mentions. Given the slender geometry of a typical foam film, a lubrication flow with a Poiseuille-type profile across the film thickness then arises (further details can be found in prior work [85–87] and in the supplementary material). Within this Poiseuille profile, flow on the film surface is opposite in direction to flow along the centre line of the film. Here though, we focus just on the film surface, because we are interested solely in surfactant that is adsorbed on the film surface, and that is then transported just by the surface flow.

In the case of a stretched film, Marangoni flow on the surface is from a region of low surface tension and hence high surfactant surface concentration Γ (namely from the edge of the film at the Plateau border) to a region of high surface tension and hence low surfactant surface concentration Γ (the region that is depleted of surfactant away from the edge). The Marangoni flow acts to mitigate the effect of the film surface having been depleted, and the Plateau border acts as a surfactant source, at least for a stretched film as in Fig. 1(a). A film that is shrinking (Fig. 1(b)) behaves in an analogous fashion, but surfactant now accumulates on the film, so surfactant surface concentration is high there. The Marangoni flow on the surface is then towards the Plateau border, and the Plateau border itself acts as a sink.

Once we know the flow velocity on the surface, we can also write down a surfactant flux. A standard conservation equation then follows, i.e. the temporal rate of change of surfactant surface concentration Γ is the negative of the divergence of the surfactant flux: this conservation equation is described next.

2.4. Governing equation

In what follows we first explain how to non-dimensionalise the system under consideration (Section 2.4.1). Then we discuss boundary and initial conditions in dimensionless form (Section 2.4.2). After that we present the surfactant conservation equation again in dimensionless form (Sections 2.4.3–2.4.4).

2.4.1. Non-dimensionalisation

Here we aim to write equations in dimensionless form. Film half-lengths and also the coordinate along the film are non-dimensionalised based on film half-length L_0 at the initial instant prior to any stretching or shrinking being imposed. Film half-thicknesses are non-dimensionalised based on film half-thickness δ_0 at that same instant. A typical value of L_0 (such as might be found in a microfluidic model porous medium [4,5]) is 10^{-3} m, and a typical value of δ_0 is 5×10^{-8} m (see the supplementary material for details, considering data from literature [95]).

Velocities on the film (and likewise film stretch rates) are non-dimensionalised based on a typical Marangoni velocity scale u_0. Details of how to compute u_0 are given in the supplementary material. A typical value of u_0 is estimated as $2\times10^{-3}\,\mathrm{m\,s^{-1}}$ (see the supplementary material which uses data compiled in prior work [86] utilising various literature sources [95,96]). This is also a velocity that would be achievable in experiments with a microfluidic model such as that described e.g. in prior work [5].

Regarding other variables, times are non-dimensionalised based on L_0/u_0, a typical value being 0.5 s, reiterating here that values of L_0 and u_0 are comparable with scales encountered experimentally in the microfluidic model used in previous studies [4,5]. Surfactant surface concentrations are non-dimensionalised based on surface concentration at the Plateau border $\Gamma_{\mathrm{Pb}*}$, a typical value being $4.6 \times 10^{-6}\,\mathrm{mol\,m^{-2}}$ (again see the supplementary material; data have been compiled in prior work [86] using information from literature [97]). A summary of all the various values that are considered typical is provided in Table S 1. Note however that different experimental set ups can have parameters that deviate from these typical values (as we will see in Section 4).

In what follows x denotes a dimensionless coordinate along the film (for simplicity, just a single coordinate direction along the film surface is treated [85–87]; by assumption there is no motion out of the plane of Fig. 1), t denotes dimensionless time, L denotes dimensionless film half-length, $\dot{L}$ denotes dimensionless rate of change of film half-length, i.e. dimensionless stretch rate (or dimensionless shrinking rate in the event that $\dot{L}$ is negative), and Γ denotes dimensionless surface concentration.

2.4.2. Boundary and initial conditions

We have a boundary condition that $\Gamma = 1$ when $x = L$, i.e. the Plateau border, acting here as a reservoir, retains its surfactant concentration. Clearly though this is a moving boundary, since L is varying: this is novel compared to prior work [85–87] which did not face the issue of a moving boundary. To proceed, it is convenient to define a new set of independent variables (X, T) in place of (x, t). We define $X = x/L$ and $T = t$. Whereas x is spatial coordinate non-dimensionalised with respect to initial film half-length, X is non-dimensionalised with respect to instantaneous film half-length. The boundary condition is now $\Gamma = 1$ at $X = 1$ (at the Plateau border), and we also have $\partial\Gamma/\partial X = 0$ at $X = 0$ (applicable on symmetry grounds at the centre of the film surface which is itself located along the centre line of the pore).

The initial condition at $T = 0$ is $\Gamma = 1$, i.e. initial equilibrium between the film and Plateau border surfaces prior to any stretch or shrinkage: note however that the system considered in prior work [85–87] had a different initial condition with films being leaner in surfactant than Plateau borders were (see the supplementary material for details of how the present initial condition is novel compared to that aforementioned prior work).

2.4.3. Surfactant conservation equation and velocity fields

The governing differential equation we seek in dimensionless form (see the derivation in the supplementary material) can be obtained starting from a surfactant conservation equation

$$\frac{\partial \Gamma}{\partial t} = -\frac{\partial (u_s \Gamma)}{\partial x} \tag{1}$$

where u_s is a dimensionless velocity along the surface, and hence the product $u_s\Gamma$ is a dimensionless flux along the surface. In the interests of simplicity as already alluded to, surfactant is assumed confined to the surface here, with negligible amounts present in the bulk. This simplification is formally the limit of an insoluble surfactant [85], but is also relevant for surfactants with finite solubility in sufficiently thin films [86,87]. The dimensionless surface velocity u_s can be written as the sum of a stretching or shrinkage term u_{sS} and a Marangoni term u_{sM}. In dimensionless form

$$u_{sS} = x\, L^{-1}\, \mathrm{d}L/\mathrm{d}t \tag{2}$$

and

$$u_{sM} = -(3L)^{-1} \partial \log \Gamma / \partial x \tag{3}$$

(dimensional analogues are given in the supplementary material). Note that the L^{-1} factor in Eq. (3) is associated with film thickness [85]. This factor arises because as films stretch, they also become thinner. However as films become thinner, a given Marangoni stress manages to deliver less flow.

Based on Eq. (3), the Marangoni-driven contribution to surfactant flux $u_{sM}\Gamma$ is simply $u_{sM}\Gamma = -(3L)^{-1}\partial\Gamma/\partial x$. Involving as it does a spatial gradient of surface concentration Γ, mathematically this has the same form as a diffusive flux, even though it arises from Marangoni convection, not from molecular diffusion. Indeed molecular diffusion in the direction along the surface, even though it can in principle occur [98], is not included in Eq. (1): this is because it is typically much weaker than any Marangoni contribution [85–87]. Further indications

of how this Marangoni term manages to behave analogous to a diffusion term and what the corresponding diffusivity represents are given in the supplementary material (see section S 1.2). Similar phenomena (i.e. diffusive-like behaviours which do not formally originate from molecular diffusion) are also known to arise in the field of suspension mechanics [99–101].

One feature of Eq. (3) that then feeds into Eq. (1) however is that it involves a simplifying assumption of a constant Gibbs elasticity (i.e. a constant derivative of surface tension with respect to logarithm of surface concentration, see the supplementary material for more information). That may be a poor assumption in the extreme limits of either a strongly stretched film surface (which would become completely denuded of surfactant) or else a strongly contracted film surface (which becomes completely packed with surfactant): the Marangoni contribution from Eq. (3) may be rather limited in those cases. Such complications are neglected here, although we revisit the possibility of Gibbs elasticity not being constant in Section 4.

Substituting Eqs. (2)–(3) into Eq. (1) results in a single equation for surfactant surface concentration Γ (see equation (S 10) in supplementary material). This equation is discussed further below.

2.4.4. Surfactant conservation equation in rescaled coordinates

It is convenient to convert equation (S 10) from (x,t) to (X,T) coordinates: see Eqs. (S 14)–(S 15) for details of how derivatives transform. Ultimately we obtain

$$\frac{\partial \Gamma}{\partial T} = -\frac{\dot{L}}{L}\Gamma + \frac{1}{3L^3}\frac{\partial^2 \Gamma}{\partial X^2} \tag{4}$$

which is the equation of main interest. Here we suppose

$$L = 1 + \dot{L}\,T. \tag{5}$$

We are therefore treating $\dot{L}$ as being constant over time, corresponding to a film moving along a constant taper pore at a constant velocity, with $\dot{L} > 0$ for stretching and $\dot{L} < 0$ for shrinking. In what follows we will consider cases with $|\dot{L}|$ ranging from values rather larger than unity (physically this implies stretching/shrinking is nominally faster than Marangoni, i.e. faster than the typical velocity scale mentioned earlier) to values rather smaller than unity (stretching/shrinking slower than Marangoni).

We identify that in Eq. (4) the first term on the right hand side represents the stretching or shrinking and the second term on the right hand side represents the Marangoni effect. The stretching/shrinking term considered here is novel compared to prior work [85–87], since the analogous term in prior work could only ever have one sign, and was constrained to be small in magnitude. Note that the Marangoni term involves a second order spatial derivative, and so (as already noted, and also elaborated upon within section S 1.2) behaves like diffusion even though diffusion itself is not formally included in the model (along the surface, molecular diffusion is much weaker than the Marangoni term, as already mentioned [85–87]). Of course, the Marangoni flow u_{sM} in Eq. (3) and hence the Marangoni flux $u_{sM}\Gamma$ involve a first order spatial derivative. The second order spatial derivative in Eq. (4) arises naturally upon taking the divergence of the surfactant flux. Note that the fact that this term is linear in surfactant surface concentration Γ relies on the aforementioned assumption of having a constant Gibbs elasticity.

The Marangoni term within Eq. (4) contains a prefactor $(3L^3)^{-1}$, which acts as an "effective" diffusion coefficient, at least for the particular dimensionless scaling used in Eq. (4). The factor $\frac{1}{3}$ comes from integrating over the aforementioned Poiseuille profile. A factor L^{-2} arises from second order spatial differentiation, remembering that $\partial/\partial x = L^{-1}\partial/\partial X$: this indicates that in terms of the variable x at least, gradients tend to be smaller when L is larger. An additional factor L^{-1} arises from the observation that (for a given Marangoni stress), surface velocity is slower when the film is thinner. However to conserve liquid in the film, the dimensionless film half-thickness δ must equal the reciprocal of dimensionless film half-length L^{-1}: remember here that half-thickness and half-length are non-dimensionalised with respect to their initial values.

We analyse the governing Eq. (4) further in the sections that follow.

2.5. Spatially uniform case and role of boundary condition

Initially the surface concentration Γ is uniform and hence the derivative $\partial^2\Gamma/\partial X^2$ is negligible. Eq. (4) then predicts a spatially uniform but time-varying solution denoted Γ_{unif}

$$\Gamma \approx \Gamma_{\text{unif}} \equiv L^{-1} \tag{6}$$

independently of coordinate X. According to this approximate solution at least, stretched films can become depleted of surfactant as film half-length L grows, which might then be detrimental to foam film stability, and could lead to foam films breaking.

The problem with this approximate solution is that it does not respect the boundary condition $\Gamma = 1$ at $X = 1$. Information about this boundary condition must therefore start to impact the solution for surfactant surface concentration Γ in some way, leading to spatial gradients in surface concentration and hence Marangoni flows. Early on, the boundary condition should only ever affect the region close to $X = 1$, with the remainder of the domain continuing to evolve as $\Gamma \approx L^{-1}$ as per Eq. (6). Over time however that situation can change.

The extent to which information about the boundary condition propagates into the solution domain, and thereby the extent to which values of surfactant surface concentration Γ inside the domain deviate from the reciprocal of film half-length L^{-1}, depends on the relative size of the two terms on the right hand side of Eq. (4). The ratio of these terms (stretching/shrinking divided by Marangoni) is $3L^2\dot{L}\,\Gamma/(\partial^2\Gamma/\partial X^2)$.

Note the prefactor here $3L^2\dot{L}$ which gives an indication of the relative size of stretching/shrinking terms and Marangoni terms, at least to the extent that surface concentration Γ and the derivative $\partial^2\Gamma/\partial X^2$ are assumed to be order unity quantities. The same conclusion can be reached directly from an analysis of the surface velocities given in Eqs. (2)–(3): the stretching/shrinking velocity u_{sS} is clearly on the order of $\dot{L}$, whereas the Marangoni velocity u_{sM} is expected to be on the order of $(3L^2)^{-1}$. This factor $(3L^2)^{-1}$ itself arises from a combination of two effects. First of all, longer films have smaller gradients of $\log\Gamma$ along them (at least in terms of coordinate x as in Eq. (3)). Secondly, longer films are also thinner and so have lower velocities on them [85]. Hence the ratio u_{sS}/u_{sM} (stretching/shrinking to Marangoni) is estimated nominally as $3L^2\dot{L}$, subject to the assumption that Γ and $\partial^2\Gamma/\partial X^2$ are order unity quantities. Of course this quantity $3L^2\dot{L}$ is given in dimensionless form here: an analogous quantity in dimensional form is described in section S 1.2. If the magnitude of $3L^2\dot{L}$ is small, then we expect that the Marangoni term will influence the solution significantly, as we discuss next.

2.6. Quasistatic solution

In this limit of small $3L^2\dot{L}$, it turns out (see the supplementary material section S 2 for details) that the system approaches a quasistatic solution Γ_{QS} (with the left hand side of Eq. (4) then becoming negligible). In the stretching case, this state satisfies

$$\Gamma \approx \Gamma_{QS} \equiv \frac{\cosh((3L^2\dot{L})^{1/2}X)}{\cosh((3L^2\dot{L})^{1/2})}. \tag{7}$$

In the shrinking case we have instead

$$\Gamma \approx \Gamma_{QS} \equiv \frac{\cos((3L^2|\dot{L}|)^{1/2}X)}{\cos((3L^2|\dot{L}|)^{1/2})}. \tag{8}$$

Note that Eq. (7) predicts values of surfactant surface concentration Γ less than unity, whereas Eq. (8) predicts values of this quantity in excess of unity.

Of particular interest is the value of Γ at the centre of the film $X = 0$, which is the location at which Γ deviates most from unity. We denote this value Γ_c, or more particularly in the case of a quasistatic solution we denote it Γ_{QSc}. The predictions of this quantity Γ_{QSc} are in the stretching case

$$\Gamma_c \approx \Gamma_{QSc} \equiv \frac{1}{\cosh((3L^2\dot{L})^{1/2})} \equiv \operatorname{sech}((3L^2\dot{L})^{1/2}) \tag{9}$$

and in the shrinking case

$$\Gamma_c \approx \Gamma_{QSc} \equiv \frac{1}{\cos((3L^2|\dot{L}|)^{1/2})} \equiv \sec((3L^2\dot{L})^{1/2}). \tag{10}$$

Clearly for the value of Γ_c to be close to unity (or in other words for the boundary condition $\Gamma = 1$ at $X = 1$ to have significant influence over the entire film) we need the magnitude of $3L^2\dot{L}$ to be small compared to unity, as we have assumed. One way of achieving this is to have a very small magnitude for $\dot{L}$. However for a stretching case, L grows with time, so even though $3L^2\dot{L}$ might start off small, it will not remain small. On the other hand for a shrinking case, the magnitude of $3L^2\dot{L}$ will become smaller and smaller over time.

A consequence of having small magnitude for $3L^2\dot{L}$ is that, via Eqs. (7)–(8), the derivative $\partial^2\Gamma/\partial X^2$ will actually be much smaller than unity (by contrast with the naive estimate for the value of $\partial^2\Gamma/\partial X^2$ previously made in Section 2.5). This is however what manages within Eq. (4) to keep Marangoni flow in quasistatic balance with stretching/shrinking flows in the present limit.

2.7. Boundary layer case

In the stretching case, in the limit when L is large ($L \gg 1$), and likewise $3L^2\dot{L}$ is large, we cannot seek a quasistatic solution, at least not over most of the film. Instead Eq. (6), which balances the left hand side of Eq. (4) (unsteady state term) with the first term on the right (stretching/shrinking term), applies over most of the film.

To satisfy the boundary condition though, we need to seek a quasistatic state albeit confined now near the Plateau border. Specifically we seek a boundary layer solution, denoted Γ_{BL}, valid within an x-domain of order unity close to $x = L$, or equivalently an X-domain of order L^{-1} close to $X = 1$. Within this boundary layer, the derivative $\partial^2\Gamma/\partial X^2$ will now be much larger than unity (again a contrast with the naive estimate in Section 2.5). The surfactant surface concentration Γ turns out to be (see the supplementary material section S 2)

$$\Gamma \approx \Gamma_{BL} \equiv \operatorname{erfc}((3L^2\dot{L}/2)^{1/2}(1-X))\exp((3L^2\dot{L}/2)(1-X)^2). \tag{11}$$

This satisfies as required $\Gamma = 1$ when $X = 1$. Note that erfc is a rapidly decreasing function of its argument, whereas exp is a rapidly increasing function of its argument. The net effect however for large values of $(3L^2\dot{L}/2)^{1/2}(1-X)$ turns out to be a decay, as can be derived from standard asymptotic formulae for erfc at large values of its argument [102]

$$\Gamma_{BL} \sim \frac{1}{(3\pi L^2\dot{L}/2)^{1/2}(1-X)}. \tag{12}$$

The fact that the boundary solution Γ_{BL} decays as the value of $1 - X$ increases is consistent with joining up with a uniform solution $\Gamma \approx \Gamma_{\text{unif}} \equiv L^{-1} \ll 1$ far from the boundary, remembering the assumption that $L \gg 1$ here.

2.8. Numerical approach

To summarise, Eqs. (6)–(12) constitute asymptotic predictions for how surfactant surface concentration on either stretching or shrinking foam films should behave under various limiting circumstances. More generally however, numerical solutions are required. Indeed our purpose here is to solve the surfactant evolution Eq. (4) numerically, and then to compare the numerical solutions with the above asymptotic ones. A Crank–Nicolson method [103] has been employed here to solve Eq. (4). Details of the method (including level of spatial discretisation, time step size and benchmarking) are given in the supplementary material (section S 3). Results are presented next.

3. Results

In this results section, model predictions for stretched films are considered in Sections 3.1–3.2 and for shrinking films are considered in Sections 3.3–3.4. Some additional results are presented in the supplementary material (section S 4).

3.1. Profiles of surfactant surface concentration: Stretched films

Fig. 2 shows profiles of surfactant surface concentration Γ versus spatial coordinate X for various film half-length L values ($L = 2$, 4 and 16) and various stretch rates $\dot{L}$ ($\dot{L} = \frac{1}{64}$, $\frac{1}{8}$, 1 and 4). Note that we have chosen to plot profiles at specific L values, but this corresponds via Eq. (5) to well-defined times. What we see is that increasing film half-length L causes the value of Γ to decrease.

Starting with Fig. 2(a), which has a comparatively small stretch rate $\dot{L} = \frac{1}{64}$, it is evident that over the entire profile, the value of Γ departs comparatively little from unity, at least for $L = 2$ and $L = 4$. This indicates that the boundary condition $\Gamma = 1$ at $X = 1$ is having a strong effect on the profile, so that Marangoni flow is effective at delivering surfactant from the Plateau border onto the film. Certainly, at $L = 2$ and $L = 4$, the value of Γ is significantly in excess of the uniform value $\Gamma_{\text{unif}} \equiv L^{-1}$ (see Eq. (6)) which would otherwise have been obtained in the absence of any Marangoni effect. For $L = 16$ meanwhile, the amount that the surfactant surface concentration Γ departs from unity is noticeably larger than what is observed for $L = 2$ or $L = 4$. However the value of Γ still remains significantly in excess of L^{-1}.

Consulting Fig. 2(b), Fig. 2(c) and Fig. 2(d), we observe that increasing film stretch rate $\dot{L}$ causes the surfactant surface concentration Γ to decrease, at any given L. In Fig. 2(c) we do see the value of Γ approaching L^{-1}, although for $L = 2$ and $L = 4$, this occurs only near the centre of the film $X = 0$. For $L = 16$ though, the value of Γ approaches L^{-1} over a wider domain. In Fig. 2(d) meanwhile, even when $L = 2$ and $L = 4$, there is a significant domain of X for which the value of Γ is close to L^{-1}. This widens further when $L = 16$.

One way to understand better the various profiles in Fig. 2 is to compare them with the asymptotic predictions in Sections 2.6 and 2.7. In Fig. 3 for instance, we see that when $L = 2$ and $\dot{L} = \frac{1}{64}$ there is reasonably good agreement between the computed value of Γ and the quasistatic prediction Γ_{QS} via Eq. (7): as the figure shows, there is an absolute difference of no more than about 0.01 between them. We have mentioned that the quasistatic solution is predicted to perform better when the parameter $3L^2\dot{L}$ is small. Increasing film half-length L at fixed stretch rate $\dot{L}$ means that agreement is less close than before (see Figure S 2(a) in supplementary material). On the other hand decreasing $\dot{L}$ at fixed L leads to even closer agreement (see Figure S 2(b) in supplementary material).

For large values of $3L^2\dot{L}$, we no longer expect agreement between the computed surface concentration Γ and the quasistatic formula Γ_{QS}. Instead we expect the surface concentration Γ to be around a uniform value $\Gamma_{\text{unif}} \equiv L^{-1}$ away from the boundary (as Fig. 2 already shows), and to obey a boundary layer formula Γ_{BL} (see Eq. (11)) close to the boundary. Fig. 4 shows cases with $L = 4$ and $L = 16$, in each case with both $\dot{L} = 1$ and $\dot{L} = 4$ being considered. There is indeed a reasonably good fit to the boundary layer formula, but the case with $L = 16$ exhibits a better fit than the case with $L = 4$. This improved fit follows because the formula for Γ_{BL} is predicted to decay moving far from the boundary (see Eq. (12)). Even though the actual surfactant surface concentration Γ stops decaying spatially away from the boundary and instead eventually reaches a limiting value of L^{-1}, this limiting value is itself small provided the film half-length L is large. Another observation from Fig. 4 is that for larger values of $3L^2\dot{L}$, the boundary layer becomes compressed nearer to $X = 1$. This is in line with predictions from Eq. (11).

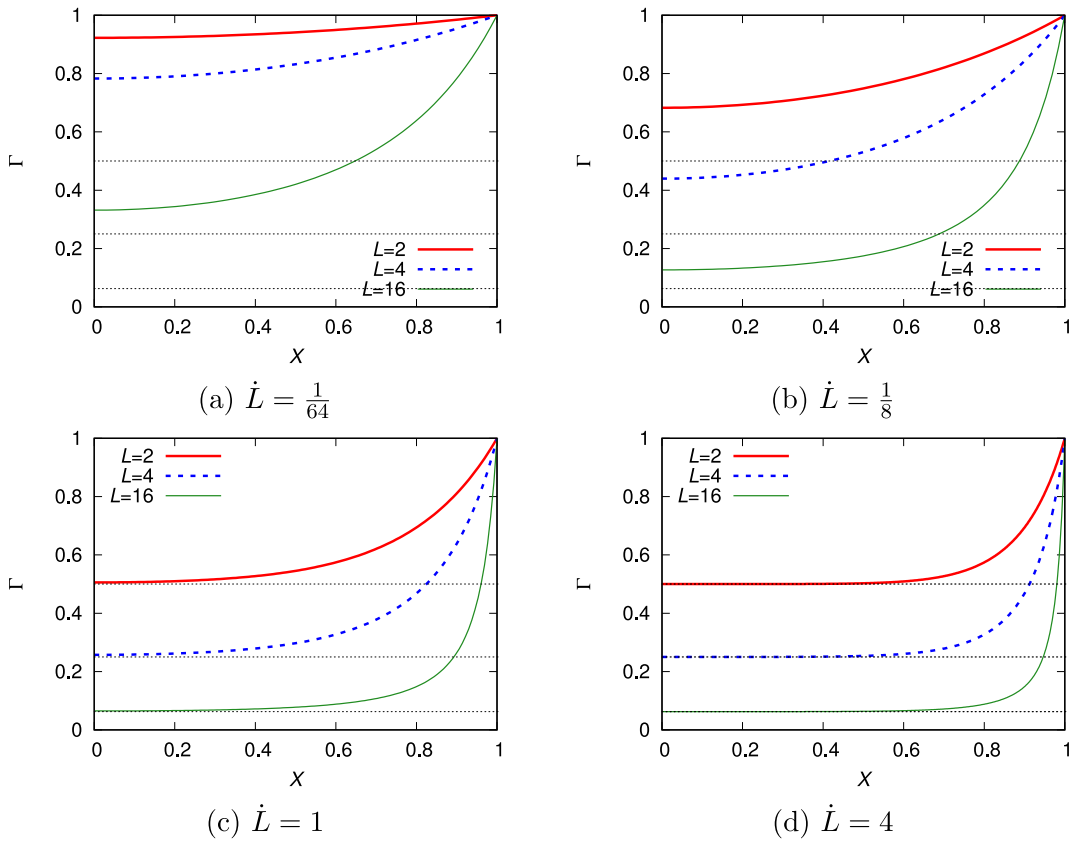

Fig. 2. Surfactant surface concentration Γ vs coordinate X, for various film half-lengths L ($L = 2$, 4 and 16) and various film stretch rates $\dot{L}$. The horizontal dotted lines show the values of L^{-1}.

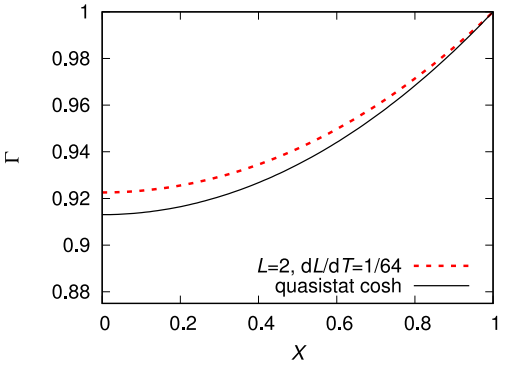

Fig. 3. Comparison between surfactant surface concentration Γ vs coordinate X profile (for $L = 2$ and $\dot{L} = \frac{1}{64}$) and quasistatic formula, which involves cosh functions (see Eq. (7)).

3.2. Evolution of surfactant surface concentration: Stretched films

Fig. 2 through Fig. 4 discussed above show snapshots of Γ versus X just at particular instants, i.e. just at particular L values. It is also of interest to consider how the surfactant surface concentration Γ (or more particularly the value Γ_c at the centre of the film) evolves as a function of film half-length L. This is what Fig. 5 shows for various $\dot{L}$ values, i.e. various stretching rates.

In all cases the value of surfactant surface concentration at the centre Γ_c is initially unity. Early on, the evolution of Γ_c as a function of L is actually the same for all $\dot{L}$ values. This is because initially the spatial derivative $\partial^2\Gamma/\partial X^2$ vanishes, and the solution of Eq. (4) then reduces to Eq. (6). When $\dot{L}$ is small however (e.g. $\dot{L} = \frac{1}{64}$), the value of Γ_c starts to depart from the prediction of Eq. (6) after just a modest increment of L. Thereafter, the decrease of Γ_c is comparatively slow. Increasing the stretch rate $\dot{L}$ to a value $\dot{L} = \frac{1}{8}$ say, gives a faster decay of Γ_c with respect to L. Increasing further to $\dot{L} = 1$ gives an even faster decay. However increasing beyond that to $\dot{L} = 4$ has barely any further impact on the evolution of Γ_c.

In Fig. 6 we compare plots of surfactant surface concentration at the centre Γ_c versus film half-length L with various asymptotic formulae. In Fig. 6(a) we compare with the prediction of Eq. (9) (which involves a hyperbolic secant), and supposing $\dot{L} = \frac{1}{64}$. We see agreement up to around $L = 2$ (consistent with what Fig. 3 shows), but after that, Eq. (9) is an underestimate of the actual value of Γ_c. This is unsurprising as a hyperbolic secant is a very rapidly decaying function of its argument. Indeed we only expect Eq. (9) to be reliable for small values of the argument. A reduction in stretching rate $\dot{L}$ would make Eq. (9) reliable over a wider domain of film half-length L (see Figure S 3 in the supplementary material which shows this for the case $\dot{L} = \frac{1}{256}$).

In Fig. 6(b) meanwhile we consider the value of Γ_c versus L for $\dot{L} = 1$. It agrees very well with the prediction of Eq. (6), i.e. the value of Γ_c is very close to $\Gamma_{\text{unif}} \equiv L^{-1}$. The boundary condition, namely $\Gamma = 1$ at $X = 0$, is having essentially no impact on Γ_c, and this situation will not change if stretch rate $\dot{L}$ increases further to $\dot{L} = 4$ say (as Fig. 5 already showed).

3.3. Profiles of surfactant surface concentration: Shrinking films

Now we switch from stretching films to shrinking ones. Data for surfactant surface concentration Γ versus coordinate X are presented in Fig. 7. We consider values of film half-length L equal to $\frac{1}{2}$, $\frac{1}{4}$ and $\frac{1}{8}$. Meanwhile we consider values of shrinking rate $\dot{L}$ equal to $-\frac{1}{8}$, -1 and -4. We do not consider even smaller values of L (e.g. $L = \frac{1}{16}$). Neither do we consider even smaller values of $|\dot{L}|$ (e.g. we do not consider

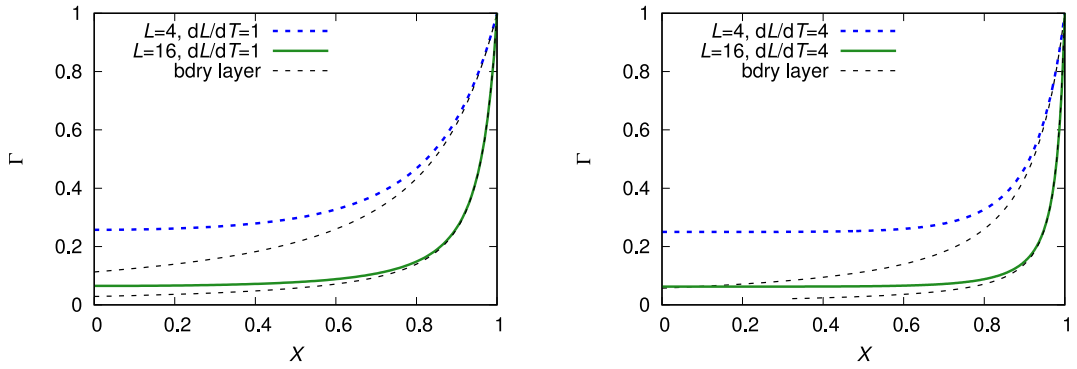

(a) $L = 4$ or $L = 16$; $\dot{L} = 1$ (b) $L = 4$ or $L = 16$; $\dot{L} = 4$

Fig. 4. Comparison between surfactant surface concentration Γ vs coordinate X profile (for various film half-lengths L and various stretch rates $\dot{L}$) and boundary layer profiles (see Eq. (11)), which are applicable near the Plateau border (close to $X = 1$).

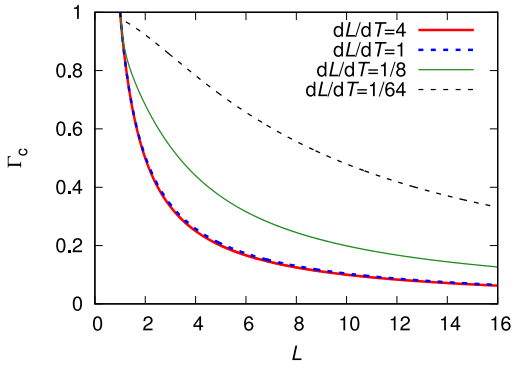

Fig. 5. Surfactant surface concentration at the centre of the film Γ_c vs film half-length L for various $\dot{L}$.

$\dot{L} = -\frac{1}{64}$). The reason is that small values of the parameter $3L^2|\dot{L}|$ are expected to be sufficient to ensure near quasistatic behaviour for the surface concentration Γ: small values of this can already be obtained with $L = \frac{1}{8}$ and $\dot{L} = -\frac{1}{8}$ say.

Consulting Fig. 7 we observe that values of Γ now exceed unity (during shrinking) rather than being below unity (as was the case with stretching). Nonetheless, for $\dot{L} = -\frac{1}{8}$, Fig. 7(a) shows that the value of Γ is only ever slightly above unity, and the amount by which it exceeds unity decays as L decreases from $\frac{1}{2}$ to $\frac{1}{4}$ to $\frac{1}{8}$ (see also Figure S 4(a) in supplementary material for a comparison with the approximate formula in Eq. (8)). Clearly the boundary condition $\Gamma = 1$ at $X = 1$ has a strong impact on these profiles.

Switching to $\dot{L} = -1$ in Fig. 7(b), we see a bigger deviation from unity than before. However the impact of the aforementioned boundary condition at $X = 1$ is still significant. Without that boundary condition, we would have surface concentrations $\Gamma \approx \Gamma_{\text{unif}} \equiv L^{-1}$, so the case with $L = \frac{1}{2}$ would have $\Gamma \approx 2$. Clearly though that value is far from being attained in Fig. 7(b). Smaller L values (e.g. $\frac{1}{4}$ or $\frac{1}{8}$) moreover return the value of Γ back towards unity.

In Fig. 7(c) with $\dot{L} = -4$, we do see the $L = \frac{1}{2}$ case approaching $\Gamma \approx 2$, but only near $X = 0$. What is evident in Fig. 7(c) however is that the surface concentration Γ continues increasing even when the film half-length L falls below $L = \frac{1}{2}$. As a consequence, the case with $L = \frac{1}{4}$ can attain even higher values of Γ than the $L = \frac{1}{2}$ case does. That said, a value as large as L^{-1} is never attained when $L = \frac{1}{4}$, so the boundary condition is definitely having impact here. Once we reach $L = \frac{1}{8}$, the value of Γ has fallen back to a level much closer to unity.

3.4. Evolution of surfactant surface concentration: Shrinking films

In Fig. 8 we plot surface concentration at the centre of the film Γ_c as a function of film half-length L for various values of $\dot{L}$, all of them with $\dot{L} < 0$. Note that since L is shrinking here, the time evolution of the system corresponds to moving from right to left. For the reasons already mentioned in Section 3.3 we consider L values down to $L = \frac{1}{8}$ but no smaller. Likewise we consider values of $|\dot{L}|$ down to $|\dot{L}| = \frac{1}{8}$ but no smaller.

Note the non-monotonic behaviour of Γ_c (which is distinct from the monotonic behaviours seen in the stretching case). In Fig. 8, for each $\dot{L}$, the value of Γ_c rises from unity (the initial condition), attains a peak value, and then falls back towards unity. Values of Γ_c close to unity are expected for small enough L (in particular when $3L^2|\dot{L}|$ is much smaller than unity), since the system should then attain a quasistatic state, and surface concentration at the centre Γ_c can then never depart much from the condition $\Gamma = 1$ at $X = 1$ imposed on the boundary.

Also plotted in Fig. 8 is the function $\Gamma_{\text{unif}} = L^{-1}$. All the curves (with different $\dot{L}$) follow this for at least some domain of L values below $L = 1$ (moving from right to left in the figure). The curve with the highest $|\dot{L}|$ (i.e. $\dot{L} = -4$) follows it the furthest, until roughly $L \approx \frac{1}{2}$. However for L values any smaller than that, the value of Γ_c deviates from L^{-1}.

In an attempt to explain the shape of the surfactant surface concentration at the centre Γ_c versus film half-length L curves for smaller L values, we consider the quasistatic formula (Eq. (10)), which involves a secant function. We plot this in Fig. 9: remember that film half-length L evolves from right to left in this figure. In Fig. 9(a) with $\dot{L} = -\frac{1}{8}$, we see good agreement between the numerically computed value of Γ_c and Eq. (10) for any L values less than around $\frac{1}{2}$. In Fig. 9(b), with $\dot{L} = -1$, we require smaller L values (below around $\frac{1}{4}$) before agreement is seen. Switching to even larger values of $|\dot{L}|$ (with $\dot{L} = -4$; see Figure S 4(b) in the supplementary material) agreement is only seen around $L \approx \frac{1}{8}$ (and presumably for smaller L values also, although we do not explore L values any smaller than that here).

4. Preliminary comparison with experiment

In this section we make a preliminary comparison between predictions of the model that is developed in the present work and experiments reported in literature. We consider the case of imposed stretching as there tends to be more experimental work in literature on stretching of films [63–65] (as opposed to shrinking them). Such experimental work is often motivated by interest in measuring how stable foam films can be upon stretching [67–69] and also interest in producing giant films [104] possibly up to the order of metres in size.

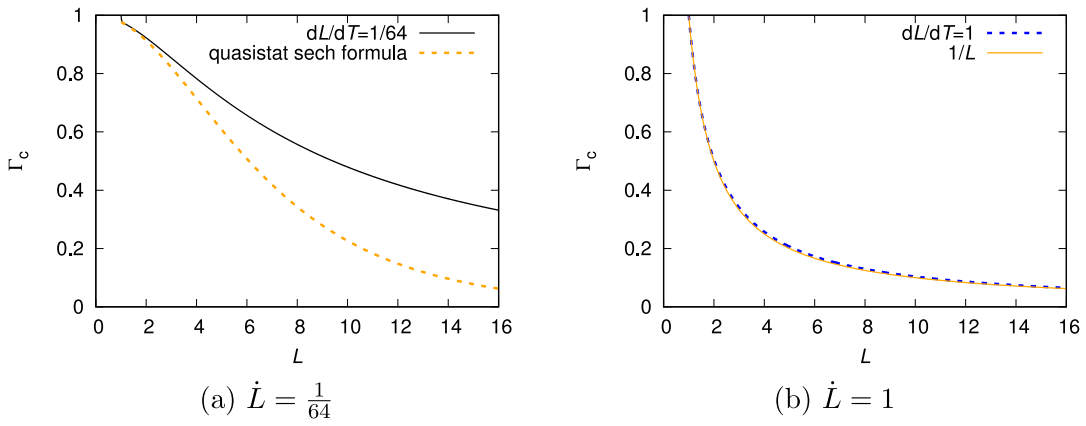

Fig. 6. Comparison between surfactant surface concentration at the centre Γ_c vs film half-length L and either the quasistatic formula (which involves sech functions, see Eq. (9)) or else the spatially uniform formula (which involves L^{-1}, see Eq. (6)).

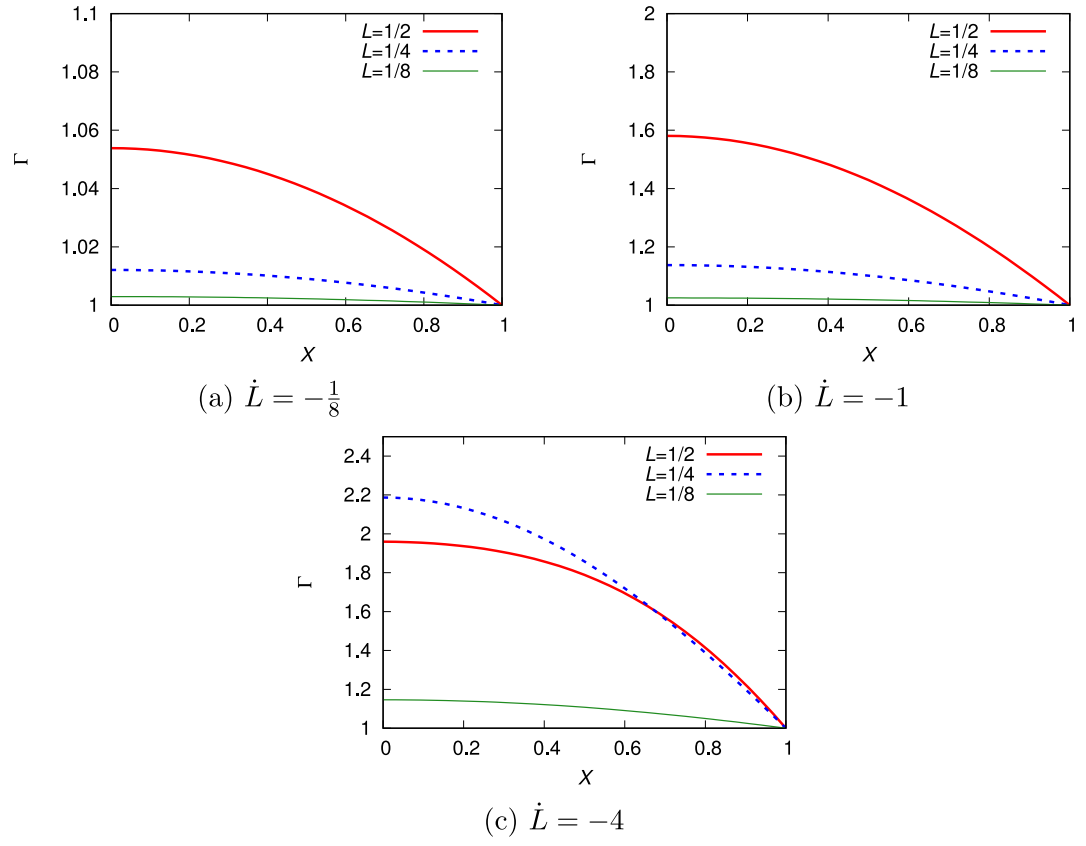

Fig. 7. Surfactant surface concentration Γ vs coordinate X, for various film half-lengths L ($L = \frac{1}{2}$, $\frac{1}{4}$ and $\frac{1}{8}$) and various shrinking rates $\dot{L}$.

The literature experiments we analyse here [93] consider however films of a more modest size (up to around 10^{-2} m). Specifically they involve a circular soap film that is suspended between two other films, which are catenoid shaped [105] and each of which is attached to a circular wire ring. The circular soap film is necessarily smaller in radius than the wire rings. Moving the wire rings closer together however causes the radius of the soap film to grow, i.e. the film is stretched. In what follows we describe relevant experimental parameter values (Section 4.1), film elongation and extraction (Section 4.2), and imposed film stretch rates (Section 4.3). Then in Section 4.4 we discuss, for specified stretch rates, the amount of stretch that can be imposed upon a film, up to the point at which new film begins to be extracted from an adjacent Plateau border meniscus: model predictions and experimental data are compared. As we will see, there is at least qualitative agreement between model and experiment here, but there are also restrictions upon the parameter regime for which such comparisons can be made.

4.1. Parameter values relevant to experiments

Before proceeding we describe the dimensional parameters relevant to the experiments discussed here [93], which differ somewhat from often encountered typical scales reported in Table S 1 in supplementary material. Specifically the wire rings had radius 1.1×10^{-2} m, and their motion changed the soap film radius from 7×10^{-3} m to 10^{-2} m. In the dimensionless model considered in the present work, this corresponds to a final dimensionless film half-length L with a value of $L \approx 1.43$.

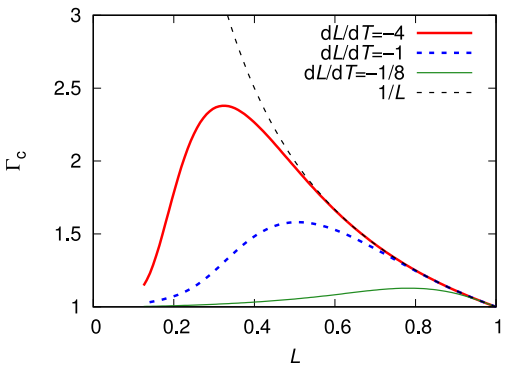

Fig. 8. Surfactant surface concentration at the centre of the film Γ_c vs film half-length L for various $\dot{L}$. Note that since $\dot{L}$ is negative, the time evolution involves moving from right to left here. The spatially uniform formula (which involves L^{-1}, see Eq (6)) is also shown.

Returning to consider the experiments, film thicknesses were also measured [93] and were found to be on the order of 10^{-6} m (so that film half-thickness is 5×10^{-7} m).

During the experiments, the wire rings were moved towards one another at various speeds [93] from 0.05×10^{-3} m s^{-1} to 50×10^{-3} m s^{-1}. We estimate that as a result (see section S 5.1 in supplementary material for more explanation), the Plateau border meniscus at the edge of the soap film moved at a speed which was between 0.03×10^{-3} m s^{-1} to 30×10^{-3} m s^{-1}. Using the reported values [93] of viscosity 1.4×10^{-3} Pa s and of equilibrium surface tension 35×10^{-3} N m^{-1}, this can be expressed as a dimensionless capillary number Ca, with values in the domain 1.2×10^{-6} to 1.2×10^{-3}.

4.2. Film elongation and film extraction

It is however necessary to relate these capillary numbers Ca to a (dimensionless) imposed film stretch rate $\dot{L}$, which is the parameter that appears in the model developed in the present work. When attempting to establish such a relationship, one of the issues identified experimentally is that sometimes only part of the meniscus motion produces elongation within the film. The remainder of the meniscus motion causes extraction of new film from the meniscus itself. In the experiments, extracted film is rather thicker than originally existing film, so is easily distinguished [93]. It was claimed [93] that the film would elongate only up until the point that the relative change in surface tension (i.e. change in surface tension divided by equilibrium surface tension) was equal to $3.8\,Ca^{2/3}$.

This value $3.8\,Ca^{2/3}$ was obtained via so called Frankel theory [106,107] which demands a velocity-dependent increase in surface tension in order to extract film from a Plateau border meniscus. Since Ca was itself a small parameter, there was an indication that significant film stretch (without accompanying extraction) could only be achieved using surfactants of very low surface elasticity (much smaller than elasticities for typical surfactant systems as quoted in Table S 1). Thus for the experiments discussed here [93], a particular surfactant system was selected with exceptionally low elasticity: the Gibbs elasticity was estimated as 10^{-3} N m^{-1} or less.

4.3. Domain of film stretch rates

The above parameter set now gives us sufficient information to relate capillary number Ca and dimensionless imposed stretch rate $\dot{L}$ (see section S 5.2 in supplementary material for explanation of how they are related). The result for the experimental system discussed here [93] is $\dot{L} = 5 \times 10^5\, Ca$ or equivalently $Ca = 2 \times 10^{-6}\, \dot{L}$. Given the set of Ca values already mentioned earlier, it then follows that $\dot{L}$ for the experiments is in the domain $1.2 \leq \dot{L} \leq 1200$. In the context of the model developed in the present work, most of the domain of $\dot{L}$ explored thereby corresponds to rapid stretch (large $\dot{L}$).

The present model would then predict (see Sections 2.5, 3.1 and 3.2) a dimensionless surface concentration $\Gamma \sim L^{-1}$. The change in $\log L$ during stretching thereby gives the change in $\log \Gamma$. However the change in $\log \Gamma$ then tells us the change in dimensionless surface tension on the film, a result which follows by definition of the Gibbs elasticity, supposing that the surface tension has itself been made dimensionless based on Gibbs elasticity.

4.4. Stretching to the point of film extraction

Recall that, prior to any film extraction happening, the relative increase in surface tension on the film could be up to $3.8\,Ca^{2/3}$. This value is however taken relative to equilibrium tension. The analogous value taken relative to Gibbs elasticity (for the experimental system currently under discussion [93]) would be $133\,Ca^{2/3}$ or equivalently $0.0211\,\dot{L}^{2/3}$.

Experimental data are available [93] for how the value of $L - 1$ (the change in film half-length relative to initial film half-length) that is needed to commence extracting new film varies as a function of capillary number Ca or equivalently as a function of imposed stretch rate $\dot{L}$. What the experimental data show [93] is that the value of $L - 1$ required to commence extraction is an increasing function of Ca or equivalently of $\dot{L}$. The model used in the present work predicts an analogous sort of behaviour at least qualitatively, giving a relation $\log L \approx 0.0211\,\dot{L}^{2/3}$ or equivalently $L - 1 \approx -1 + \exp(0.0211\,\dot{L}^{2/3})$. Observe that the model used in the present work, despite not incorporating any film extraction, can still be used to predict the point at which extraction might onset.

Remember from Section 4.1 that the experimental study [93] involves stretching the dimensionless film half-length L up to $L \approx 1.43$. Thus $L - 1 \approx 0.43$ or equivalently $\log L \approx 0.353$. To have any film extracted up to and including this particular L value, the model used in the present work requires $\dot{L}$ to be no greater than about 70, or equivalently Ca to be no greater than about 1.4×10^{-4}. Selecting this specific Ca value and examining experimental data [93] (noting also comments about the data made in section S 5.3), we find $L - 1$ values (at the point of film extraction) varying from about 0.09 to 0.6 depending on the exact surfactant formulation used. The present model predicts, as we have said, a value $L - 1 \approx 0.43$ which lies within the observed experimental range.

One reason why the model predictions and experiments might differ is that the model assumes Gibbs elasticity remains constant independent of film stretch. On the other hand, the experiments corresponding to onset of film extraction at lower values of $L - 1$ (e.g. values around 0.09 as mentioned above) start off with comparatively low Gibbs elasticity (much smaller than equilibrium surface tension) but Gibbs elasticity then rises sharply beyond a certain level of stretch [93]. Surface tension rises likewise, and this then promotes film extraction after comparatively little additional stretch. Another reason for differences here between model and experiment arises from geometry: the model assumes stretching along one dimension only, whereas the experiments involve biaxial stretch of a circular film. In a biaxial system, surfactant surface concentration Γ falls more rapidly with increasing film half-length L than is the case in one dimension. Again this promotes film extraction even at more modest values of L.

In summary, the model employed here does capture qualitatively some of the observations from experimental work [93]. However since the model considers only film elongation (not film extraction) there are restrictions on its use, either to systems with rather limited imposed stretch or else to systems with large imposed stretch but low Gibbs elasticity (which must be much lower than equilibrium surface tension). One comment we make though, is that the experimental work [93] seems to have focussed on relatively large values of the stretch rate

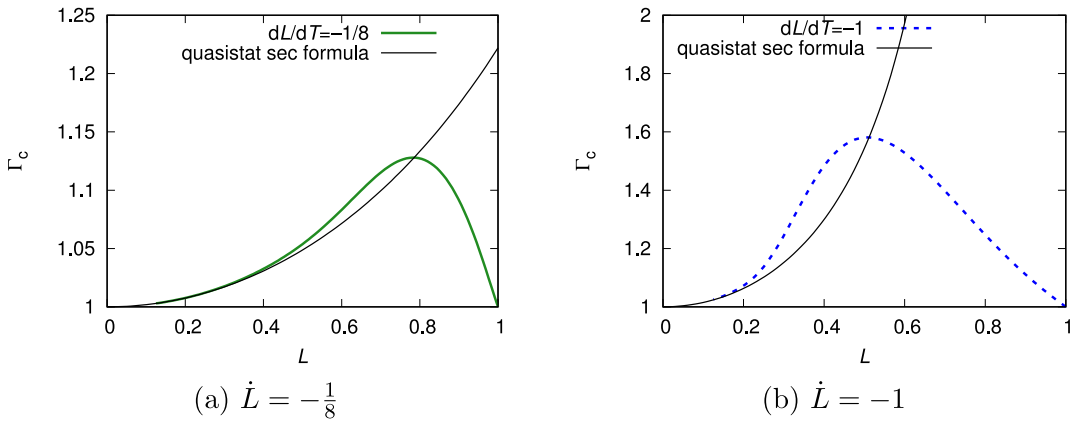

Fig. 9. Comparison between surfactant surface concentration at the centre Γ_c vs film half-length L and the quasistatic formula, which involves sec functions, see Eq. (10).

parameter $\dot{L}$. For much smaller values of $\dot{L}$, the change in surface tension up to any specified film half-length would be predicted to be much smaller, at least according to the model considered here: a Taylor expansion of Eq. (9) would predict a dimensionless change in surface tension of around $3L^2\dot{L}/2$. This is linear in $\dot{L}$. For very small $\dot{L}$, it might then be difficult the attain the level of surface tension needed to extract new film which itself scales proportional to $\dot{L}^{2/3}$.

5. Conclusions

We have presented a simple model for surfactant transport on foam films as films travel through a porous medium. In the model, films can either stretch (travelling from pore throat to pore body) or shrink (travelling from pore body to pore throat). The model itself has been adapted from the field of foam fractionation [85–87]. Although film stretching or shrinking is not so relevant in the context of fractionation, film thinning is relevant, and is closely analogous to stretching. That then is why an analogous model can be employed here, albeit the analogy has not been explored previously.

In the present context, high stretch rates lead to predictions of films becoming highly depleted in surfactant. The higher the stretch rate and also the higher the amount of stretch (relative to the initial film half-length), the more likely it is that the film will become depleted. Surfactant can be supplied to stretched films via Plateau borders located at the edges of films where they meet pore walls: there can be rather more liquid in the Plateau borders than in the films themselves. According to the model, whether or not Plateau borders are effective at delivering surfactant onto films depends on the product of the stretch rate (compared to a characteristic Marangoni velocity) and the square of the film half-length (relative to initial half-length). Identifying the role of this product, and its physical interpretation (namely an estimated nominal ratio between stretching-driven and Marangoni-driven flows) has been a novel contribution of the present work. When this product is small, the influence of the Plateau borders is expected to be felt over the entire film. When the product is large however (and it becomes larger as the film stretches over time), the effect of the Plateau border is felt only in a boundary layer, and the surfactant surface concentration in the rest of the film can keep falling over time independently of the Plateau border.

Surfactant surface concentration upon films that shrink is predicted to behave differently from those that stretch. Shrinkage on its own implies that surfactant tends to accumulate on shrinking films, but Plateau borders now also act as a surfactant sink. Again the relevant parameter is the product of a rate (now a shrinkage rate) and the square of a film half-length. This parameter falls over time, indicating Plateau borders become increasingly effective as sinks. Non-monotonic behaviour is now expected for surfactant surface concentration, with surfactant first accumulating on films and later being restored to surface concentrations compatible with conditions in Plateau borders. The expected evolution of surfactant surface concentration in the stretched case by contrast is monotonic.

Returning to the stretched case, we reiterate that high stretch rates (or indeed high relative amounts of stretch for a particular stretch rate) can lead to films becoming highly depleted of surfactant. If films become sufficiently depleted of surfactant, they may break (although breakage itself is not formally included in the model). Breakage would be detrimental to foam in porous media applications, including foam improved oil recovery, foam-based soil remediation and foam-based aquifer remediation. What the model might guide us upon is how rapidly a foam film could be driven along a pore without being at risk of surfactant surface concentration falling sufficiently low that breakage might occur. The model would also seem to indicate that porous media with large ratios of pore body size to pore throat size might be those within which films are most at risk of breaking. However that risk could be mitigated by driving the foam films more slowly still.

Of course there are many simplifications contained within the model as it stands, and definitive predictions of flows that arise and associated surfactant transport leading to foam film breakage would rely on more sophisticated modelling, such as various prior studies have considered [48,72,90,91]. One significant issue with the model is that under stretching it considers only existing films that become elongated, not extraction of new film from Plateau borders: even though the model includes a mechanism for surfactant transport from Plateau border to film, any accompanying transport of liquid is not considered. In fact experiment shows [93] (at least for the set of stretch rates explored) that extraction of new film can be significant, unless the amount of stretch imposed is limited and/or the Gibbs elasticity of the film is low (much lower than an equilibrium surface tension say). Nonetheless as a tool to sketch out a possible operating envelope with comparatively little effort, the present model potentially will prove useful.

As well as summarising what has been achieved here, it is also worth reflecting upon what still needs to be achieved in the future. This study has presented a model which can predict comparatively simply, how surfactant surface concentration could behave on foam films moving through a porous medium. The present work has not however tested that model against experiment, at least not experiment in a porous medium scenario. Previous work on foam in porous media indicates that surfactant concentration should influence foam film stability [38, 57], but to complete the model and compare with experiment, the exact relation between surfactant surface concentration and film stability would also need to be established. Whilst simplicity of the model used here is part of its appeal, that same simplicity also dictates the outlook for how the model might be most effectively tested experimentally For example, the sketch in Fig. 1 envisages a film moving along a tapered pore with that pore being symmetric about its centre line.

Such symmetry might not be seen in a naturally occurring porous medium, but would be easy to set up in a micromodel [4–8]. Hence for experimental tests of the model described herein, it is recommended to deal in the first instance with experiments on engineered porous media, e.g. micromodel systems.

CRediT authorship contribution statement

Paul Grassia: Conceptualization, Formal analysis, Funding acquisition, Investigation, Methodology, Software, Supervision, Validation, Visualization, Writing – original draft. **Hamed Rajabi:** Formal analysis, Investigation, Methodology, Software, Writing – review & editing. **Ruben Rosario:** Formal analysis, Investigation, Methodology, Software, Writing – review & editing. **Carlos Torres-Ulloa:** Formal analysis, Writing – review & editing.

Declaration of competing interest

The authors declare that they have no known competing financial interests or personal relationships that could have appeared to influence the work reported in this paper.

Data availability

The full set of data actually analysed herein have been tabulated and supplied as supplementary material raw data. These data are also available via https://doi.org/10.15129/2a588cdd-68a5-45c7-b267-dd15243bc5a3.

Acknowledgements

P. Grassia and C. Torres-Ulloa acknowledge funding from EPSRC, United Kingdom grant EP/V002937/1. H. Rajabi acknowledges funding from a Faculty of Engineering International Scholarship from University of Strathclyde, United Kingdom. R. Rosario acknowledges funding from a Strathclyde Research Studentship from University of Strathclyde, United Kingdom. C. Torres-Ulloa acknowledges support from the Centro de Investigación, Innovación y Creación (CIIC), Universidad Católica de Temuco.

Appendix A. Supplementary data

Supplementary material related to this article can be found online at https://doi.org/10.1016/j.colsurfa.2023.132575.

References

[1] A.R. Kovscek, C.J. Radke, Fundamentals of foam transport in porous media, in: L.L. Schramm (Ed.), Foams: Fundamentals and Applications in the Petroleum Industry, in: Advances in Chemistry, vol. 242, American Chemical Society, Washington, DC, 1994, pp. 115–163, Ch. 3.

[2] B. Géraud, S.A. Jones, I. Cantat, B. Dollet, Y. Méheust, The flow of a foam in a two-dimensional porous medium, Water Resour. Res. 52 (2016) 773–790, http://dx.doi.org/10.1002/2015WR017936.

[3] A. Telmadarreie, J.J. Trivedi, Post-surfactant CO_2 foam/polymer-enhanced foam flooding for heavy oil recovery: Pore-scale visualization in fractured micromodel, Transp. Porous Media 113 (2016) 717–733, http://dx.doi.org/10.1007/s11242-016-0721-z.

[4] K. Osei-Bonsu, P. Grassia, N. Shokri, Investigation of foam flow in a 3-D printed porous medium in the presence of oil, J. Colloid Interf. Sci. 490 (2017) 850–858, http://dx.doi.org/10.1016/j.jcis.2016.12.015.

[5] K. Osei-Bonsu, P. Grassia, N. Shokri, Effects of pore geometry on flowing foam dynamics in 3D-printed porous media, Transp. Porous Media 124 (2018) 903–917, http://dx.doi.org/10.1007/s11242-018-1103-5.

[6] M.J. Shojaei, K. Osei-Bonsu, P. Grassia, N. Shokri, Foam flow investigation in 3D-printed porous media: Fingering and gravitational effects, Ind. Engng Chem. Res. 57 (2018) 7275–7281, http://dx.doi.org/10.1021/acs.iecr.8b00136.

[7] S.A. Jones, N. Getrouw, S. Vincent-Bonnieu, Foam flow in a model porous medium: I. The effect of foam coarsening, Soft Matter 14 (2018) 3490–3496, http://dx.doi.org/10.1039/C7SM01903C.

[8] S.A. Jones, N. Getrouw, S. Vincent-Bonnieu, Foam flow in a model porous medium: II. The effect of trapped gas, Soft Matter. 14 (2018) 3497–3503, http://dx.doi.org/10.1039/C7SM02458D.

[9] K. Li, K.-H.A.A. Wolf, W.R. Rossen, Effects of gas trapping on foam mobility in a model fracture, Transp. Porous Media 138 (2021) 185–200, http://dx.doi.org/10.1007/s11242-021-01598-y.

[10] K. Li, K.-H.A.A. Wolf, W.R. Rossen, A novel technique to estimate water saturation and capillary pressure of foam in model fractures, Colloids Surf. A, Physicochem. Engg. Aspects. 632 (2022) 127800, http://dx.doi.org/10.1016/j.colsurfa.2021.127800.

[11] P. Johnson, V. Starov, A. Trybala, Foam flow through porous media, Curr. Opin. Colloid Interface Sci. 58 (2022) 101555, http://dx.doi.org/10.1016/j.cocis.2021.101555.

[12] R. Farajzadeh, H. Bertin, W.R. Rossen, Editorial to the special issue: Foam in porous media for petroleum and environmental engineering: Experience sharing, Transp. Porous Media 131 (2020) 1–3, http://dx.doi.org/10.1007/s11242-019-01329-4.

[13] W.R. Rossen, Foams in enhanced oil recovery, in: R.K. Prud'homme, S.A. Khan (Eds.), Foams: Theory, Measurements and Applications, in: Surfactant Science Series, Marcel Dekker, New York, 1996, pp. 99–187, Ch. 2.

[14] D. Shan, W.R. Rossen, Optimal injection strategies for foam IOR, SPE J. 9 (2004) 132–150, http://dx.doi.org/10.2118/88811-PA.

[15] R. Farajzadeh, A. Andrianov, R. Krastev, G.J. Hirasaki, W.R. Rossen, Foam-oil interaction in porous media: Implications for foam assisted enhanced oil recovery, Adv. Coll. Interface Sci. 183–184 (2012) 1–13, http://dx.doi.org/10.1016/j.cis.2012.07.002.

[16] P. Grassia, E. Mas-Hernández, N. Shokri, S.J. Cox, G. Mishuris, W.R. Rossen, Analysis of a model for foam improved oil recovery, J. Fluid Mech. 751 (2014) 346–405, http://dx.doi.org/10.1017/jfm.2014.287.

[17] K. Ma, G. Ren, K. Mateen, D. Morel, P. Cordelier, Modeling techniques for foam flow in porous media, SPE J. 20 (2015) 453–470, http://dx.doi.org/10.2118/169104-PA.

[18] M. Eneotu, P. Grassia, Foam improved oil recovery: Towards a formulation for pressure-driven growth with flow reversal, Proc. R. Soc. Lond. Ser. A Math. Phys. Eng. Sci. 476 (2020) 20200573, http://dx.doi.org/10.1098/rspa.2020.0573.

[19] C. Torres-Ulloa, P. Grassia, Foam propagation with flow reversal, Transp. Porous Media 147 (2023) 629–651, http://dx.doi.org/10.1007/s11242-023-01925-5.

[20] S.-W. Jeong, M.Y. Corapcioglu, A micromodel analysis of factors influencing NAPL removal by surfactant foam flooding, J. Contam. Hydrol. 60 (2003) 77–96, http://dx.doi.org/10.1016/s0169-7722(02)00054-2.

[21] C.N. Mulligan, F. Eftekhari, Remediation with surfactant foam of PCP-contaminated soil, Eng. Geol. 70 (2003) 269–279, http://dx.doi.org/10.1016/S0013-7952(03)00095-4.

[22] S. Wang, C.N. Mulligan, An evaluation of surfactant foam technology in remediation of contaminated soil, Chemosphere 57 (2004) 1079–1089, http://dx.doi.org/10.1016/j.chemosphere.2004.08.019.

[23] H.J. Couto, G. Massarani, E.C. Biscaia, G.L. Santa-Anna, Remediation of sandy soils using surfactant solutions and foams, J. Hazard. Mater. 164 (2009) 1325–1334, http://dx.doi.org/10.1016/j.jhazmat.2008.09.129.

[24] L. Zhong, J.E. Szecsody, F. Zhang, S.V. Mattigod, Foam delivery of amendments for vadose zone remediation: Propagation performance in unsaturated sediments, Vadose Zone J. 9 (2010) 757–767, http://dx.doi.org/10.2136/vzj2010.0007.

[25] M. Longpré-Girard, R. Martel, T. Robert, R. Lefebvre, J.-M. Lauzon, 2D sandbox experiments of surfactant foams for mobility control and enhanced LNAPL recovery in layered soils, J. Contam. Hydrol. 193 (2016) 63–73, http://dx.doi.org/10.1016/j.jconhyd.2016.09.001.

[26] H. Bertin, E. Del Campo Estrada, O. Atteia, Foam placement for soil remediation, Environ. Chem. 14 (2017) 338–343, http://dx.doi.org/10.1071/EN17003.

[27] M. Longpré-Girard, R. Martel, T. Robert, R. Lefebvre, J.-M. Lauzon, N. Thomson, Surfactant foam selection for enhanced light non-aqueous phase liquids (LNAPL) recovery in contaminated aquifers, Transp. Porous Media 131 (2020) 65–84, http://dx.doi.org/10.1007/s11242-019-01292-0.

[28] R. Aranda, H. Davarzani, S. Colombano, F. Laurent, H. Bertin, Experimental study of foam flow in highly permeable porous media for soil remediation, Transp. Porous Media 134 (2020) 231–247, http://dx.doi.org/10.1007/s11242-020-01443-8.

[29] H. Davarzani, R. Aranda, S. Colombano, F. Laurent, H. Bertin, Experimental study of foam propagation and stability in highly permeable porous media under lateral water flow: Diverting groundwater for application to soil remediation, J. Contam. Hydrol. 243 (2021) 103917, http://dx.doi.org/10.1016/j.jconhyd.2021.103917.

[30] T. Føyen, B. Brattekås, M.A. Fernø, A. Barrabino, T. Holt, Increased CO_2 storage capacity using CO_2-foam, Int. J. Greenh. Gas Control 96 (2020) 103016, http://dx.doi.org/10.1016/j.ijggc.2020.103016.

[31] W.R. Rossen, R. Farajzadeh, G.J. Hirasaki, M. Amirmoshiri, Potential and challenges of foam-assisted CO_2 sequestration, in: SPE Improved Oil Recovery Conference, Virtual, 25th–29th Apr. 2022, -MS, http://dx.doi.org/10.2118/209371.

[32] P. Dong, M. Puerto, G. Jian, K. Ma, K. Mateen, G. Ren, G. Bourdarot, D. Morel, M. Bourrel, S.L. Biswal, G. Hirasaki, Low-IFT foaming system for enhanced oil recovery in highly heterogeneous/fractured oil-wet carbonate reservoirs, SPE J. 23 (2018) 2243–2259, http://dx.doi.org/10.2118/184569-PA.
[33] P. Ghosh, K.K. Mohanty, Study of surfactant alternating gas injection (SAG) in gas-flooded oil-wet, low permeability carbonate rocks, Fuel 251 (2019) 260–275, http://dx.doi.org/10.1016/j.fuel.2019.03.119.
[34] T. Blaker, M.G. Aarra, A. Skauge, L. Rasmussen, H.K. Celius, H.A. Martinsen, F. Vassenden, Foam for gas mobility control in the Snorre field: The FAWAG project, SPE Reserv. Eval. Engg. 5 (2002) 317–323, http://dx.doi.org/10.2118/78824-PA.
[35] P.A. Gauglitz, F. Friedmann, S.I. Kam, W.R. Rossen, Foam generation in homogeneous porous media, Chem. Eng. Sci. 57 (2002) 4037–4052, http://dx.doi.org/10.1016/S0009-2509(02)00340-8.
[36] Z.I. Khatib, G.J. Hirasaki, A.H. Falls, Effects of capillary pressure on coalescence and phase mobilities in foams flowing through porous media, SPE Reserv. Eng. 3 (1988) 919–926, http://dx.doi.org/10.2118/15442-PA.
[37] A.R. Kovscek, T.W. Patzek, C.J. Radke, A mechanistic population balance model for transient and steady-state foam flow in Boise sandstone, Chem. Eng. Sci. 50 (1995) 3783–3799, http://dx.doi.org/10.1016/0009-2509(95)00199-F.
[38] A.R. Kovscek, T.W. Patzek, C.J. Radke, Mechanistic foam flow simulation in heterogeneous and multidimensional porous media, SPE J. 2 (1997) 511–526, http://dx.doi.org/10.2118/39102-PA.
[39] R.F. Li, W. Yan, S. Liu, G.J. Hirasaki, C.A. Miller, Foam mobility control for surfactant enhanced oil recovery, SPE J. 15 (2010) 928–942, http://dx.doi.org/10.2118/113910-PA.
[40] K. Ma, J.L. Lopez-Salinas, M.C. Puerto, C.A. Miller, S.L. Biswal, G.J. Hirasaki, Estimation of parameters for the simulation of foam flow through porous media, Part 1: The dry-out effect, Energy Fuels 27 (2013) 2363–2375, http://dx.doi.org/10.1021/ef302036s.
[41] A.I. Jiménez, C.J. Radke, Dynamic stability of foam lamellae flowing through a periodically constricted pore, in: J.K. Borchardt, T.F. Yen (Eds.), Oil-Field Chemistry: Enhanced Recovery and Production Stimulation, in: ACS Symposium Series, (no. 396) American Chemical Society, Washington, 1989, pp. 460–479, Ch. 25.
[42] W.R. Rossen, Minimum pressure gradient for foam flow in porous media: Effect of interactions with stationary lamellae, J. Colloid Interf. Sci. 139 (1990) 457–468, http://dx.doi.org/10.1016/0021-9797(90)90118-8.
[43] W.R. Rossen, Theory of mobilization pressure gradient of flowing foams in porous media: I. Incompressible foam, J. Colloid Interf. Sci. 136 (1990) 1–16, http://dx.doi.org/10.1016/0021-9797(90)90074-X.
[44] W.R. Rossen, Theory of mobilization pressure gradient of flowing foams in porous media: III. Asymmetric lamella shapes, J. Colloid Interf. Sci. 136 (1990) 38–53, http://dx.doi.org/10.1016/0021-9797(90)90076-Z.
[45] S.J. Cox, S. Neethling, W.R. Rossen, W. Schleifenbaum, P. Schmidt-Wellenburg, J.J. Cilliers, A theory of the effective yield stress of foam in porous media: The motion of a soap film traversing a three-dimensional pore, Colloids Surf. A, Physicochem. Engg. Aspects 245 (2004) 143–151, http://dx.doi.org/10.1016/j.colsurfa.2004.07.004.
[46] D.J. Ferguson, S.J. Cox, The motion of a foam lamella traversing an idealised bi-conical pore with a rounded central region, Colloids Surf. A, Physicochem. Engg. Aspects 438 (2013) 56–62, http://dx.doi.org/10.1016/j.colsurfa.2013.02.015.
[47] H. Zhang, P.R. Brito-Parada, S.J. Neethling, Y. Wang, Yield stress of foam flow in porous media: The effect of bubble trapping, Colloids Surf. A, Physicochem. Engg. Aspects 655 (2022) 130246, http://dx.doi.org/10.1016/j.colsurfa.2022.130246.
[48] P. Stewart, S. Davis, S. Hilgenfeldt, Viscous Rayleigh-Taylor instability in aqueous foams, Colloids Surf. A, Physicochem. Engg. Aspects 436 (2013) 898–905, http://dx.doi.org/10.1016/j.colsurfa.2013.08.021.
[49] P.S. Stewart, S.H. Davis, S. Hilgenfeldt, Microstructural effects in aqueous foam fracture, J. Fluid Mech. 785 (2015) 425–461, http://dx.doi.org/10.1017/jfm.2015.636.
[50] P.S. Stewart, S. Hilgenfeldt, Gas-liquid foam dynamics: From structural elements to continuum descriptions, Annu. Rev. Fluid Mech. 55 (2023) 323–350, http://dx.doi.org/10.1146/annurev-fluid-032822-125417.
[51] O.G. Apaydin, A.R. Kovscek, Surfactant concentration and end effects on foam flow in porous media, Transp. Porous Media 43 (2001) 511–536, http://dx.doi.org/10.1023/A:1010740811277.
[52] S.A. Jones, G. Laskaris, S. Vincent-Bonnieu, R. Farajzadeh, W.R. Rossen, Effect of surfactant concentration on foam: From coreflood experiments to implicit-texture foam-model parameters, J. Ind. Eng Chem. 37 (2016) 268–276, http://dx.doi.org/10.1016/j.jiec.2016.03.041.
[53] G. Yu, W.R. Rossen, S. Vincent-Bonnieu, Coreflood study of effect of surfactant concentration on foam generation in porous media, Ind. Engng Chem. Res. 58 (2018) 420–427, http://dx.doi.org/10.1021/acs.iecr.8b03141.
[54] A.S. Aronson, V. Bergeron, M.E. Fagan, C.J. Radke, The influence of disjoining pressure on foam stability and flow in porous media, Colloids Surf. A, Physicochem. Engg. Aspects 83 (1994) 109–120, http://dx.doi.org/10.1016/0927-7757(94)80094-4.
[55] K. Golemanov, N.D. Denkov, S. Tcholakova, M. Vethamuthu, A. Lips, Surfactant mixtures for control of bubble surface mobility in foam studies, Langmuir 24 (2008) 9956–9961, http://dx.doi.org/10.1021/la8015386.
[56] N.D. Denkov, S. Tcholakova, K. Golemanov, K.P. Ananthpadmanabhan, A. Lips, The role of surfactant type and bubble surface mobility in foam rheology, Soft Matter 5 (2009) 3389–3408, http://dx.doi.org/10.1039/B903586A.
[57] F.F. de Paula, I. Igreja, T. Quinelato, G. Chapiro, A numerical investigation into the influence of the surfactant injection technique on the foam flow in heterogeneous porous media, Adv. Water Resour. 171 (2023) 104358, http://dx.doi.org/10.1016/j.advwatres.2022.104358.
[58] B. Keshavarzi, T. Krause, S. Sikandar, K. Schwarzenberger, K. Eckert, M.B. Ansorge-Schumacher, S. Heitkam, Protein enrichment by foam fractionation: Experiment and modeling, Chem. Eng. Sci. 256 (2022) 117715, http://dx.doi.org/10.1016/j.ces.2022.117715.
[59] P. Grassia, C. Torres-Ulloa, A model for foam fractionation with spatially varying bubble size, Chem. Eng. Sci. 281 (2023) 119163, http://dx.doi.org/10.1016/j.ces.2023.119163.
[60] B. Embley, P. Grassia, Viscous froth simulations with surfactant mass transfer and Marangoni effects: Deviations from Plateau's rules, Colloids Surf. A, Physicochem. Engg. Aspects 382 (2011) 8–17, http://dx.doi.org/10.1016/j.colsurfa.2011.01.013.
[61] P. Grassia, B. Embley, C. Oguey, A Princen hexagonal foam out of physico-chemical equilibrium, J. Rheol. 56 (2012) 501–526, http://dx.doi.org/10.1122/1.3687442.
[62] D. Vitasari, S. Cox, P. Grassia, R. Rosario, Effect of surfactant redistribution on the flow and stability of foam films, Proc. R. Soc. Lond. Ser. A Math. Phys. Eng. Sci. 476 (2020) 20190637, http://dx.doi.org/10.1098/rspa.2019.0637.
[63] S. Berg, E.A. Adelizzi, S.M. Troian, Experimental study of entrainment and drainage flows in microscale soap films, Langmuir 21 (2005) 3867–3876, http://dx.doi.org/10.1021/la047178+.
[64] L. Saulnier, F. Restagno, J. Delacotte, D. Langevin, E. Rio, What is the mechanism of soap film entrainment? Langmuir 27 (2011) 13406–13409, http://dx.doi.org/10.1021/la202233f.
[65] L. Saulnier, L. Champougny, G. Bastien, F. Restagno, D. Langevin, E. Rio, A study of generation and rupture of soap films, Soft Matter 10 (2014) 2899–2906, http://dx.doi.org/10.1039/c3sm52433g.
[66] L. Saulnier, J. Boos, C. Stubenrauch, E. Rio, Comparison between generations of foams and single vertical films: Single and mixed surfactant systems, Soft Matter 10 (2014) 5280–5288, http://dx.doi.org/10.1039/c4sm00326h.
[67] P.R. Garrett, J. Davis, H.M. Rendall, An experimental study of the antifoam behaviour of mixtures of a hydrocarbon oil and hydrophobic particles, Colloids Surf. A, Physicochem. Engg. Aspects 85 (1994) 159–197, http://dx.doi.org/10.1016/0927-7757(93)02678-8.
[68] P.R. Garrett, S.P. Wicks, E. Fowles, The effect of high volume fractions of latex particles on foaming and antifoam action in surfactant solutions, Colloids Surf. A, Physicochem. Engg Aspects 282–283 (2006) 307–328, http://dx.doi.org/10.1016/j.colsurfa.2006.01.054.
[69] L. Champougny, E. Rio, F. Restagno, B. Scheid, The break-up of free films pulled out of a pure liquid bath, J. Fluid Mech. 811 (2017) 499–524, http://dx.doi.org/10.1017/jfm.2016.758.
[70] I.B. Ivanov, K.D. Danov, P.A. Kralchevsky, Flocculation and coalescence of micron-size emulsion droplets, Colloids Surf. A, Physicochem. Engg. Aspects 152 (1999) 161–182, http://dx.doi.org/10.1016/S0927-7757(98)00620-7.
[71] K.D. Danov, D.S. Valkovska, I.B. Ivanov, Effect of surfactants on the film drainage, J. Colloid Interf. Sci. 211 (1999) 291–303, http://dx.doi.org/10.1006/jcis.1998.5973.
[72] L.Y. Yeo, O.K. Matar, E.S. Perez de Ortiz, G.F. Hewitt, The dynamics of Marangoni-driven local film drainage between two drops, J. Colloid Interf. Sci. 241 (2001) 233–247, http://dx.doi.org/10.1006/jcis.2001.7743.
[73] A. Bussonnière, E. Shabalina, M.X. Ah-Thon, Le. Fur, I. Cantat, Dynamical coupling between connected foam films: Interface transfer across the menisci, Phys. Rev. Lett. 124 (2020) 018001, http://dx.doi.org/10.1103/PhysRevLett.124.018001.
[74] A. Bussonnière, I. Cantat, Local origin of the visco-elasticity of a millimetric elementary foam, J. Fluid Mech. 922 (2021) A25, http://dx.doi.org/10.1017/jfm.2021.529.
[75] R. Poryles, T. Lenavetier, E. Schaub, A. Bussonnière, A. Saint-Jalmes, I. Cantat, Non-linear elasticity of foam films made of SDS/dodecanol mixtures, Soft Matter 18 (2022) 2046–2053, http://dx.doi.org/10.1039/D1SM01733K.
[76] P. Grassia, Surfactant transport between foam films, J. Fluid Mech. 928 (2021) F1, http://dx.doi.org/10.1017/jfm.2021.690.
[77] P. Grassia, Analysis of a model for surfactant transport around a foam meniscus, Proc. R. Soc. Lond. Ser. A Math. Phys. Eng. Sci. 478 (2022) 20220133, http://dx.doi.org/10.1098/rspa.2022.0133.
[78] R. Lemlich, Principles of foam fractionation, in: E.S. Perry (Ed.), Progress in Separation and Purification, Interscience, New York, 1968, pp. 1–56.
[79] R. Lemlich, Adsorptive Bubble Separation Techniques, Academic Press, Inc., New York, London, 1972.
[80] P.J. Martin, H.M. Dutton, J.B. Winterburn, S. Baker, A.B. Russell, Foam fractionation with reflux, Chem. Eng. Sci. 65 (2010) 3825–3835, http://dx.doi.org/10.1016/j.ces.2010.03.025.

[81] S. Hutzler, S.T. Tobin, A.J. Meagher, A. Marguerite, D. Weaire, A model system for foam fractionation, Proc. R. Soc. Lond. Ser. A Math. Phys. Eng. Sci. 469 (2013) 20120727, http://dx.doi.org/10.1098/rspa.2012.0727.
[82] S.T. Tobin, D. Weaire, S. Hutzler, Theoretical analysis of the performance of a foam fractionation column, Proc. R. Soc. Lond. Ser. A Math. Phys. Eng. Sci. 470 (2014) 20130625, http://dx.doi.org/10.1098/rspa.2013.0625.
[83] P. Stevenson, Foam Fractionation: Principles and Process Design, Taylor & Francis, Boca Raton FL, 2014.
[84] P. Grassia, Quasistatic model for foam fractionation, Chem. Eng. Sci. 275 (2023) 118721, http://dx.doi.org/10.1016/j.ces.2023.118721.
[85] D. Vitasari, P. Grassia, P.J. Martin, Surfactant transport onto a foam lamella, Chem. Eng. Sci. 102 (2013) 405–423, http://dx.doi.org/10.1016/j.ces.2013.08.041.
[86] H. Rajabi, P. Grassia, Transport of soluble surfactant on and within a foam film in the context of a foam fractionation process, Chem. Eng. Sci. 265 (2023) 118171, http://dx.doi.org/10.1016/j.ces.2022.118171.
[87] H. Rajabi, R. Rosario, P. Grassia, Transport of convected soluble surfactants on and within the foam film in the context of a foam fractionation process, Chem. Eng. Sci. 281 (2023) 119100, http://dx.doi.org/10.1016/j.ces.2023.119100.
[88] E. Rubin, D. Melech, Foam fractionation of solutions containing two surfactants in stripping and reflux columns, Can. J. Chem. Eng. 50 (1972) 748–753, http://dx.doi.org/10.1002/cjce.5450500612.
[89] I.D. Kamalanathan, P.J. Martin, Competitive adsorption of surfactant-protein mixtures in a continuous stripping mode foam fractionation column, Chem. Eng. Sci. 146 (2016) 291–301, http://dx.doi.org/10.1016/j.ces.2016.03.002.
[90] J.L. Joye, G.J. Hirasaki, C.A. Miller, Dimple formation and behavior during axisymmetrical foam film drainage, Langmuir 8 (1992) 3083–3092, http://dx.doi.org/10.1021/la00048a038.
[91] J.L. Joye, G.J. Hirasaki, C.A. Miller, Numerical simulation of instability causing asymmetric drainage in foam films, J. Colloid Interf. Sci. 177 (1996) 542–552, http://dx.doi.org/10.1006/jcis.1996.0068.
[92] P.S. Stewart, S.H. Davis, Dynamics and stability of metallic foams: Network modeling, J. Rheol. 56 (2012) 543–574, http://dx.doi.org/10.1122/1.3695029.
[93] J. Seiwert, M. Monloubou, B. Dollet, I. Cantat, Extension of a suspended soap film: A homogeneous dilatation followed by new film extraction, Phys. Rev. Lett. 111 (2013) 094501, http://dx.doi.org/10.1103/PhysRevLett.111.094501.
[94] S.P. Frankel, K.J. Mysels, On the dimpling during the approach of two interfaces, J. Phys. Chem. 66 (1962) 190–191, http://dx.doi.org/10.1021/j100807a513.
[95] D. Exerowa, A. Nikolov, M. Zacharieva, Common black and Newton film formation, J. Colloid and Interf. Sci. 81 (1981) 419–429, http://dx.doi.org/10.1016/0021-9797(81)90424-0.
[96] M. Durand, H.A. Stone, Relaxation time of the topological T1 process in a two-dimensional foam, Phys. Rev. Lett. 97 (2006) 226101, http://dx.doi.org/10.1103/PhysRevLett.97.226101.
[97] G. Nilsson, The adsorption of tritiated sodium dodecyl sulfate at the solution surface measured with a windowless, high humidity gas flow proportional counter, J. Phys. Chem. 61 (1957) 1135–1142, http://dx.doi.org/10.1021/j150555a002.
[98] H.A. Stone, A simple derivation of the time-dependent convective-diffusion equation for surfactant transport along a deforming interface, Phys. Fluids A 2 (1990) 111–112, http://dx.doi.org/10.1063/1.857686.
[99] K.A. Landman, L.R. White, Solid/liquid separations of flocculated suspensions, Adv. Colloid Interface Sci. 51 (1994) 175–246, http://dx.doi.org/10.1016/0001-8686(94)80036-7.
[100] K.A. Landman, J.M. Stankovich, L.R. White, Measurement of the filtration diffusivity $D(\phi)$ of a flocculated suspension, AIChE J. 45 (1999) 1875–1882, http://dx.doi.org/10.1002/aic.69045090.
[101] R.G. de Kretser, S.P. Usher, P.J. Scales, D.V. Boger, K.A. Landman, Rapid filtration measurement of dewatering design and optimization parameters, AIChE J. 47 (2001) 1758–1769, http://dx.doi.org/10.1002/aic.690470808.
[102] M. Abramowitz, I. Stegun, Handbook of Mathematical Functions with Formulas, Graphs, and Mathematical Tables, Dover Publications, New York, 1965.
[103] W.H. Press, S.A. Teukolsky, W.T. Vetterling, B.P. Flannery, Numerical Recipes in C: The Art of Scientific Computing, Cambridge University Press, Cambridge, 1992.
[104] M. Pasquet, F. Restagno, I. Cantat, E. Rio, Thickness profiles of giant soap films, Phys. Rev. Fluids 8 (2023) 034001, http://dx.doi.org/10.1103/PhysRevFluids.8.034001.
[105] U. Dierkes, S. Hildebrandt, F. Sauvigny, Minimal Surfaces, Springer, Berlin, Heidelberg, 2010.
[106] K.J. Mysels, K. Shinoda, S. Frankel, Soap Films: Study of their Thinning and a Bibliography, Pergamon, New York, 1959.
[107] I. Cantat, Liquid meniscus friction on a wet wall: Bubbles, lamellae and foams, Phys. Fluids 25 (2013) 031303, http://dx.doi.org/10.1063/1.4793544.